Acta Crystallographica Section F
Structural Biology and Crystallization Communications
ISSN 1744-3091

Expression, purification, crystallization and preliminary X-ray analysis of the human RuvB-like protein RuvBL1

Sabine Gorynia,[a,b]‡ Pedro M. Matias,[a]‡ Susana Gonçalves,[a,c] Ricardo Coelho,[a] Gonçalo Lopes,[a] Mónica Thomaz,[d] Martina Huber,[b] Bernard Haendler,[e] Peter Donner[b] and Maria Arménia Carrondo[a]*

[a]ITQB – Instituto de Tecnologia Química e Biológica, Universidade Nova de Lisboa, Apartado 127, 2781-901 Oeiras, Portugal, [b]Schering AG, Protein Chemistry/Enabling Technologies, 13342 Berlin, Germany, [c]ESRF, European Synchrotron Radiation Facility, 6 Rue Jules Horowitz, BP 220, F-38043 Grenoble CEDEX, France, [d]IBET – Instituto de Biologia Experimental e Tecnológica, Apartado 12, 2781-901 Oeiras, Portugal, and [e]Schering AG, Cooperate Research Oncology, 13342 Berlin, Germany

‡ These authors contributed equally to this work.

Correspondence e-mail: carrondo@itqb.unl.pt

Received 6 December 2005
Accepted 9 December 2005

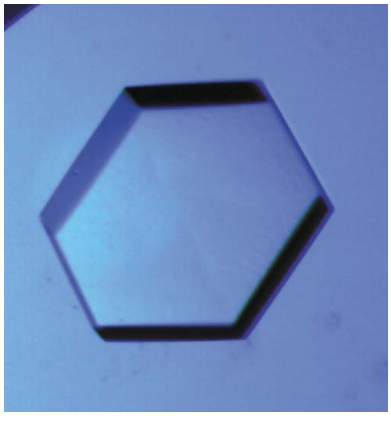

RuvBL1, an evolutionary highly conserved protein related to the AAA$^+$ family of ATPases, has been crystallized using the hanging-drop vapour-diffusion method at 293 K. The crystals are hexagonal and belong to space group *P*6, with unit-cell parameters $a = b = 207.1$, $c = 60.7$ Å and three molecules in the asymmetric unit.

1. Introduction

RuvBL1 plays important roles in transcription, DNA repair and apoptosis (Shen *et al.*, 2000; Ikura *et al.*, 2000). The protein, which is also known as TIP49a (Kanemaki *et al.*, 1997), Rvb1p (Jonsson *et al.*, 2001), TAP54α (Ikura *et al.*, 2000) and Pontin52 (Bauer *et al.*, 2000), consists of 456 amino acids and belongs to the AAA$^+$ family of ATPases (ATPase associated with diverse cellular activities; Neuwald *et al.*, 1999). For this reason, it contains a number of sequence motifs, including Walker A (P-loop) and Walker B boxes, that are involved in ATP binding and hydrolysis. The significant evolutionary conservation of RuvBL1 suggests that it mediates important cellular functions. Distinct orthologues exist in all eukaryotes as well as in archaebacteria (Makino *et al.*, 1999). A homologue of RuvBL1 has been found in the yeast INO80 chromatin-remodelling complex (Jonsson *et al.*, 2004), which is involved in transcription and DNA repair (Shen *et al.*, 2000), as well as in the human TIP60 (human immunodeficiency virus-1 Tat-interacting protein 60) HAT complex (Ikura *et al.*, 2000), which plays a role in DNA repair and apoptosis.

Jonsson and coworkers showed that Rvb1p, the yeast homologue of human RuvBL1, has widespread and complex effects on gene expression in yeast and that several cellular pathways are interrupted in a *rvb1* mutant (Jonsson *et al.*, 2001). Mutants that are unable to bind and/or hydrolyse ATP affect the transcription of over 5% of yeast genes. RuvBL1 was found to interact with c-Myc (Wood *et al.*, 2000) and has been shown to be a key modulator of apoptotic activity for both c-Myc and E2F1 (Dugan *et al.*, 2002). Additionally, RuvBL1 plays a role in the Wnt signalling pathway which regulates many important processes, such as polarity of cell division, cell proliferation and cell-fate determination, by binding to β-catenin (Bauer *et al.*, 2000; Feng *et al.*, 2003). The ATPase-deficient mutant form of RuvBL1 (D302N) inhibits β-catenin-mediated activation of TCF-dependent cellular genes (Feng *et al.*, 2003). The fact that RuvBL1 can also bind to β-catenin and LEF-1/TCF supports a role for RuvBL1 as a cofactor likely to function with diverse transcription factors.

RuvBL1 is to a large extent homologous to RuvB, the three-dimensional structure of which is already known (Putnam *et al.*, 2001; Yamada *et al.*, 2001), although the Walker A and Walker B motifs are separated by approximately 170 amino acids in RuvBL1 compared with the closely spaced motifs in RuvB. The bacterial protein RuvB functions as a motor-driving branch migration of the Holliday junction during homologous recombination (Tsaneva *et al.*, 1993).

In this paper, we describe the expression, purification, crystallization and preliminary X-ray analysis of the human RuvB-like protein RuvBL1.

2. Materials and methods

2.1. Cloning and expression

The plasmid for expression of His-FLAG-tagged RuvBL1 was constructed as follows. For separation purposes, a His_6 tag followed by a FLAG tag (MV**HHHHHHDYKDDDDK**LLV) was added to the N-terminus of RuvBL1. Firstly, the *Nco*I–*Bam*HI region was excised from pET-15b (Novagen) and replaced with the following region coding for 6×His-FLAG by using the oligonucleotide 5′-GGGCG-G*CCATGG*TTCATCACCATCACCATCACGATTACAAAGACG-ATGACGATAAACTGCTGGTTCCGCGT**GGATCC**GGTACCG-AGCTC**GCTAGC***AGATCT*GCCGGG-3′ and its complementary sequence. After annealing and digestion with *Nco*I and *Bgl*II (cutting sites are in italics), the double-stranded DNA was introduced into pET-15b. The RuvBL1 coding sequence was then PCR-amplified using the forward primer 5′-GGCCGGTT**GGATCC**AAGATCTGA-GGAGGTGAAGAGC-3′ and the reverse primer 5′-GCGCGGT-T**GCTAGC**TCACTTCATGTACTTATCCTGC-3′. The product was digested with *Bam*HI and *Nhe*I (cutting sites are in bold) and introduced downstream of the 6×His-FLAG coding region in the modified pET-15b, previously digested with the same enzymes. The resulting plasmid was sequenced for verification. The resulting His-FLAG-tagged RuvBL1 construct was used to transform *Escherichia coli* BL21 (DE3) methionine prototroph. This strain was used for production of the native RuvBL1 and the selenomethionine (SeMet) substituted RuvBL1. *E. coli* cells containing the pET-15b-RuvBL1 construct were grown overnight at 310 K in 5 ml Luria–Bertani broth supplemented with ampicillin (200 µg ml^{-1}). Cells of this preculture were harvested, washed and amplified in Overnight Express Auto-induction System 1 (Novagen) containing ampicillin at 310 K for 24 h. For production of SeMet-substituted RuvBL1, cells from the preculture were harvested and washed twice with Overnight Express Autoinduction System 2 (Novagen) containing selenomethionine (125 mg l^{-1}). The washed cells were used to inoculate 1 l of this medium lacking methionine and were grown at 310 K for 32 h at 110 rev min^{-1}.

2.2. Purification

Cells containing RuvBL1 were harvested by centrifugation (Rotor SLA-3000, Sorvall; 11 000*g* for 15 min at room temperature). The wet cells were resuspended in lysis buffer (20 m*M* Tris–HCl pH 8.0, 100 m*M* NaCl, 10% glycerol, 1 m*M* *β*-mercaptoethanol, protease-inhibitor cocktail without EDTA, Roche) and disrupted twice in a High Pressure Laboratory Homogenizer (Rannie) at 75 MPa. Soluble proteins were collected by centrifugation at 50 000*g* for 45 min. The supernatant was applied onto a 15 ml Ni–NTA Superflow (Qiagen) column which was previously equilibrated with buffer *A* (20 m*M* Tris–HCl pH 8.0, 100 m*M* NaCl, 10% glycerol, 2 m*M* *β*-mercapto-ethanol). Unbound proteins were washed out of the column using buffer *A*. RuvBL1 was eluted in a gradient (elution buffer *B*: 20 m*M* Tris–HCl pH 8.0, 100 m*M* NaCl, 10% glycerol, 2 m*M* *β*-mercapto-ethanol, 300 m*M* imidazole pH 8.0) between 40 and 100 m*M* imida-zole. The protein pool was diluted 1:2 in buffer *X* (20 m*M* Tris–HCl pH 8.0, 10% glycerol, 2 m*M* *β*-mercaptoethanol) and loaded onto a MonoQ column (Amersham Biosciences), which was equilibrated with a buffer consisting of 20 m*M* Tris–HCl pH 8.0, 10% glycerol, 50 m*M* NaCl, 2 m*M* *β*-mercaptoethanol. In a gradient with increasing NaCl concentration, RuvBL1 eluted at 200 m*M*. The peak was pooled and concentrated to a final concentration of 15 mg ml^{-1} using an Amicon Ultra Centrifugal Filter with a 30 kDa cutoff. All purification steps were monitored by SDS–PAGE analysis (not shown). Clean His-FLAG-tagged RuvBL1 was obtained after two purification steps. We first loaded the soluble *E. coli* proteins onto an Ni–NTA Super-flow column and subsequently purified RuvBL1 by anion-exchange chromatography (MonoQ column). MonoQ fractions 6–9 were pooled and concentrated.

2.3. Crystallization

The search for initial crystallization conditions was performed on a nanolitre scale using the standard conditions of the EMBL High-Throughput Crystallization Cartesian Robot (https://htxlab.embl-grenoble.fr/). The best hit was found for condition C2 of the Malonate Screen (Hampton Research) corresponding to a solution composition of 1.5 *M* sodium malonate pH 6.0 without any other additives. The results were reproducible on the microlitre scale using the same condition from Hampton and the crystals were grown within 2 d using the hanging-drop vapour-diffusion method, with a drop composition of 1.5 µl of protein solution (15 mg ml^{-1} in 20 m*M* Tris–HCl pH 8.0, 10% glycerol, 200 m*M* NaCl and 2 m*M* *β*-mercapto-

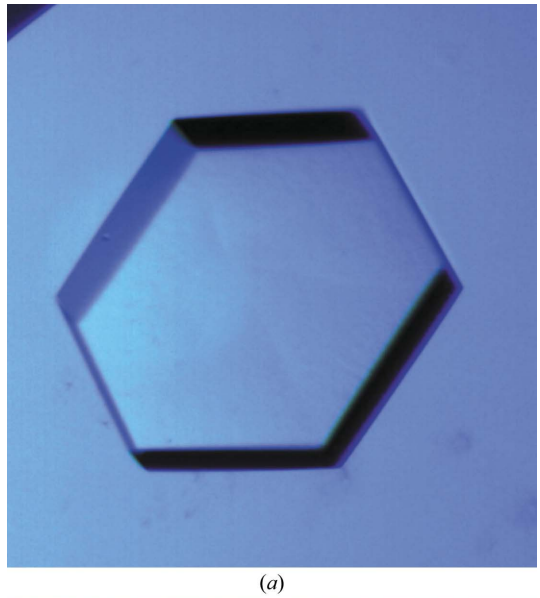

(*a*)

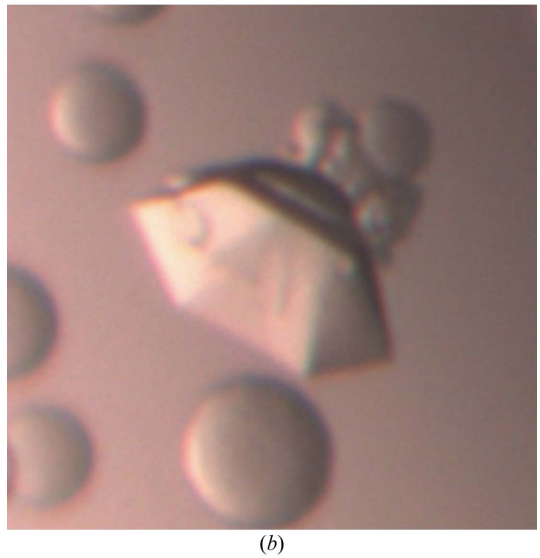

(*b*)

Figure 1
(*a*) Crystal of native RuvBL1; (*b*) crystal of SeMet-substituted RuvBL1.

ethanol) and 1.5 µl reservoir solution, equilibrated against 500 µl precipitant solution in the well. These crystals were used for the first X-ray diffraction trials. Crystallization conditions were later optimized using a gradient of increasing sodium malonate concentration at pH 6.0. The wells contained 500 µl precipitant solution and the drops were composed of 1.5 µl protein solution (15 mg ml^{-1}) and 1.5 µl reservoir solution. The best crystals were obtained from a solution containing 1.6 *M* sodium malonate pH 6 at 293 K (Fig. 1). The crystals appeared after 2 d and had dimensions of approximately 160 × 60 µm. Crystals of the SeMet derivative obtained under these conditions were used to measure diffraction data leading to the structure determination.

2.4. Data collection and preliminary crystallographic analysis

Prior to data collection, crystals were transferred into a cryoprotectant consisting of 2 *M* sodium malonate pH 6.0. All data sets were collected at the European Synchrotron Radiation Facility (ESRF) in Grenoble using CCD detectors. The main data-collection and processing statistics for three representative data sets (other data not shown) are listed in Table 1. The data sets were initially indexed, integrated, scaled and merged using the *HKL* suite (Otwinowski & Minor, 1997) and later with either *MOSFLM* (Leslie, 1992) or *XDS* (Kabsch, 1993) combined with *SCALA* in the *CCP*4 suite (Collaborative Computational Project, Number 4, 1994). The first X-ray measurements showed the RuvBL1 crystals to be sensitive to radiation damage and great care was necessary during data collection in order to minimize radiation-damage effects while at the same time measuring data to the highest possible resolution. In particular, inverse-beam geometry was used in the ID14-4 SeMet data collection to try and minimize systematic errors in anomalous differences arising from radiation damage. Also, many of the crystals investigated only diffracted to very low resolution (6 Å or less) after cryocooling. Unit-cell volume considerations indicated that the $P6_3$ crystals might contain between two and seven monomers in the asymmetric unit, corresponding to V_M (Matthews, 1968) values between 7.6 and 2.2 Å^3 Da^{-1}, with an estimated solvent content ranging between 83.8 and 43.2%. Similar considerations suggested that the *P*6 crystals might contain between one and three independent monomers, with V_M and estimated solvent-content values ranging between 7.7 and 2.6 Å^3 Da^{-1} and 83.9 and 51.6%, respectively. For all data sets, the self-rotation Patterson maps showed non-crystallographic twofold axes perpendicular to the crystallographic sixfold axis and the largest peak besides the origin in the native Patterson maps was located at coordinates (2/3, 1/3, 0) [an additional peak appears at (2/3, 1/3, 1/2) for the $P6_3$ data], suggesting the presence of non-crystallographic translational symmetry in the unit cell or a twofold NCS axis parallel to the crystallographic sixfold axis (Fig. 2).

2.5. Structure determination

Initial attempts to solve the structure by the molecular-replacement method were unsuccessful. The search models tried, chosen on the basis of sequence homology using *BLAST* (Altschul *et al.*, 1997) and with available coordinates at the Protein Data Bank (PDB; Berman *et al.*, 2000), were the RuvB molecule from *Thermotoga maritima* (PDB code 1in7; Putnam *et al.*, 2001) and the FTSH ATPase domain from *Thermus thermophilus* (PDB code 1iy1; Niwa *et al.*, 2002). These search models had a relatively low (∼30%) sequence homology with RuvBL1 and also their protein chain length differed, indicating that not all domains of RuvBL1 were represented in their three-dimensional structures.

Table 1
X-ray diffraction data-collection and processing statistics.

ESRF beamline	ID14-EH2	ID29	ID14-4
Crystal	Native	SeMet	SeMet
Detector	ADSC Quantum 4	ADSC Quantum 210	ADSC Quantum 210
Data processing	*MOSFLM*/*SCALA*	*MOSFLM*/*SCALA*†	*XDS*/*SCALA*†
Wavelength (Å)	0.933	0.9793‡	0.9791‡
Space group	$P6_3$	$P6_3$	*P*6
Unit-cell parameters (Å)			
a	207.4	207.4	207.2
c	121.5	121.5	60.77
Resolution range (Å)	30.0–2.75 (2.90–2.75)	30.0–3.0 (3.16–3.00)	45.4–2.2 (2.32–2.20)
Observations	323936	392896	612942
Unique reflections	76433	59637	73593
Completeness (%)	99.6 (97.8)	100.0 (100.0)	96.5 (80.0)
Anomalous completeness (%)	N/A	100.0 (100.0)	91.9 (66.4)
Redundancy	4.2 (3.8)	6.6 (6.6)	8.3 (3.8)
Anomalous redundancy	N/A	3.3 (3.2)	4.3 (2.2)
R_{merge}§	0.089 (0.486)	0.147 (0.797)	0.068 (0.617)
$I/\sigma(I)$	5.1 (1.5)	3.2 (0.9)	8.1 (1.2)

† Bijvoet mates were treated as non-equivalent observations for scaling and merging. ‡ Chosen with *CHOOCH* (Evans & Pettifer, 2001) as the wavelength with maximal f'' from a fluorescence scan around the Se X-ray absorption *K* edge. § $R_{merge} = \sum_{hkl}\sum_i |I_{hkl,i} - \langle I_{hkl}\rangle| / \sum_{hkl}\sum_i |I_{hkl,i}|$, where $\langle I_{hkl}\rangle$ is the mean intensity of the set of symmetry-related reflections denoted by $I_{hkl,i}$.

Heavy-atom derivative screening from native RuvBL1 crystals was likewise unsuccessful. None of the several compounds tried gave useful crystals for phasing using either the MIR, SIR, SIRAS or heavy-atom SAD methods.

The three-dimensional structure of RuvBL1 was solved using the SAD method and the ID14-4 SeMet data set. Initially, owing to the observation of NCS twofold axes in the self-rotation Patterson maps, it was assumed that there would be two RuvBL1 monomers in the asymmetric unit. Each molecule contains 12 methionine residues, but the first, located at the N-terminal of the molecule, was assumed to be either missing or disordered. Therefore, 22 Se sites were expected. Using the *HKL2MAP* graphical user interface (Pape & Schneider, 2004), the ID14-4 SeMet data set was analyzed with *SHELXC* (G. M. Sheldrick, personal communication), the heavy-atom substructure was determined with *SHELXD* (Schneider & Sheldrick, 2002) and the phase problem solved with *SHELXE* (Sheldrick, 2002). *SHELXD* found many possible solutions out of 100 trials, the best having a correlation coefficient of 50.8% and containing 29 possible selenium sites in the asymmetric unit of the crystal structure. The *SHELXE* calculations led to a clear discrimination between the correct and the inverted substructures. However, the electron-density maps were not of sufficient quality to allow interpretation and model building. The 29 selenium sites located with *SHELXD* were then input to a maximum-likelihood heavy-atom parameter refinement using *SHARP* (de La Fortelle & Bricogne, 1997). The *SHARP* calculations showed that eight of these were spurious and were therefore discarded. Thus, a total of 21 Se sites were used in the final *SHARP* calculations, followed by density modification with *SOLOMON* (Abrahams & Leslie, 1996), leading to a final correlation coefficient on $|E^2|$ of 0.688, with an optimized solvent content of 53.5%. Attempts at automated model building with *ARP*/*wARP* (Perrakis *et al.*, 1999) were unsuccessful, but a partial model was obtained showing parts of the main chain for the two expected RuvBL1 molecules in the asymmetric unit. At this stage, an inspection of the electron-density maps revealed that in each of the two RuvBL1 monomers partly built by *ARP*/*wARP* only seven of the expected 11 Se sites were visible in the electron density, with the

other four probably being located in disordered regions of the structure. The seven remaining Se sites out of the total of 21 located were seen to belong to a third monomer in the asymmetric unit. Model building of the three independent molecules is currently in progress using electron-density maps obtained from the *SHARP*/*SOLOMON* and *ARP*/*wARP* calculations. A representative series of stacked sections of the *SHARP*/*SOLOMON* electron-density map is represented in Fig. 3.

Our preliminary results suggest that RuvBL1 assembles into a hexameric structure with a central channel (Fig. 3). In the *P*6 crystal structure of RuvBL1 there are three crystallographically independent monomers related by non-crystallographic symmetry: one is located around the crystallographic sixfold axis and the other two are located around one of the two crystallographic threefold axes. By space-group symmetry, there are thus two crystallographically non-equivalent hexamers, parts of which are visible in Fig. 3. The large peaks at (2/3, 1/3, 0) visible in the $w = 0$ section of the *P*6 crystal form Patterson maps (Fig. 2*c*) result from a NCS twofold axis parallel to the crystallographic sixfold axis between the two monomers that form the second crystallographically distinct hexamer. However, there is no obvious relationship between whole monomers to explain the appearance of non-crystallographic twofolds perpendicular to the crystallographic sixfold axis, as seen in Fig. 2(*a*).

3. Concluding remarks

We have been able to solve the three-dimensional structure of the human RuvB-like protein RuvBL1 in its SeMet form from 2.2 Å diffraction data measured near the Se X-ray absorption *K* edge by using the SAD method to derive initial phases, which were then improved by density modification. Model building of the three independent molecules in the asymmetric unit is in progress, but it is anticipated that parts of the three-dimensional structure of RuvBL1 in this crystal form will be disordered, since we have already determined that four of the expected 11 ordered methionine residues in each molecule are not visible in the electron-density maps.

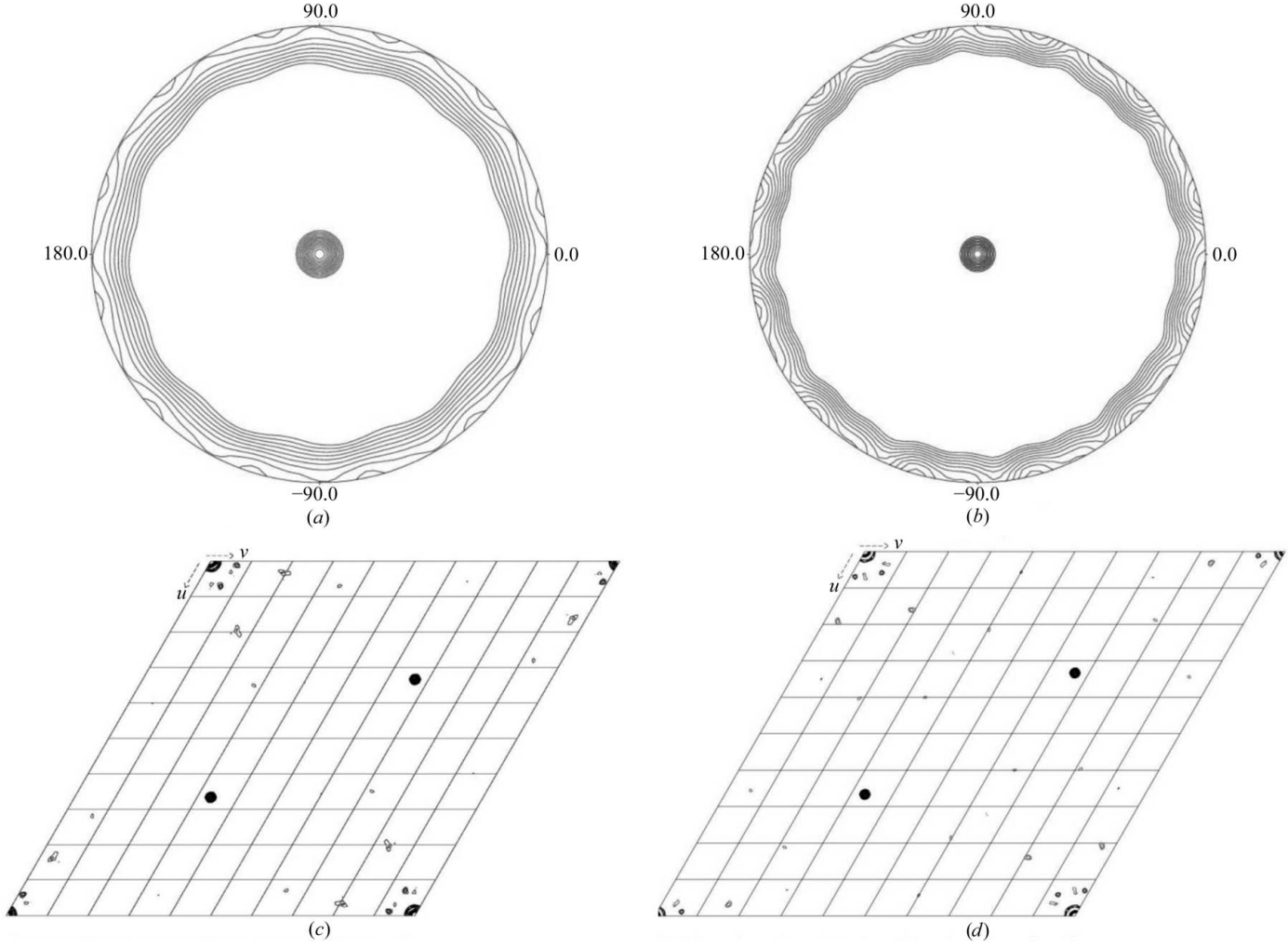

Figure 2
(*a*) $\kappa = 180^\circ$ section of the self-rotation Patterson map calculated from the ID14-EH2 ($P6_3$) data. Map calculations used an integration radius of $5 \leq R \leq 20$ Å and data in the resolution range $3.25 \leq d \leq 19.6$ Å. Data were sharpened by applying a *B* factor of -25 Å^2. The maximum value was normalized to 100 and the contours drawn at five-unit intervals starting at 40. (*b*) $\kappa = 180^\circ$ section of the self-rotation Patterson map calculated from the ID14-EH4 (*P*6) data. Map calculations used an integration radius of $5 \leq R \leq 25$ Å and data in the resolution range $3.2 \leq d \leq 20.0$ Å. Data were sharpened by applying a *B* factor of -25 Å^2. The maximum value was normalized to 100 and the contours drawn at five-unit intervals starting at 40. (*c*) $w = 0$ section of the native Patterson map calculated from the ID14-EH2 ($P6_3$) data using reflections in the resolution range $3.25 \leq d \leq 19.6$ Å with $F_{obs} \geq 3\sigma(F_{obs})$. Contour levels are drawn every 0.5 map r.m.s. units between 2.5 and 100. (*d*) $w = 0$ section of the native Patterson map calculated from the ID14-EH4 (*P*6) data using reflections in the resolution range $3.0 \leq d \leq 20.0$ Å with $F_{obs} \geq 3\sigma(F_{obs})$. Contour levels are drawn every 0.5 map r.m.s. units. Figures were prepared with the programs *NPO* and *XPLOT84DRIVER* (Collaborative Computational Project, Number 4, 1994).

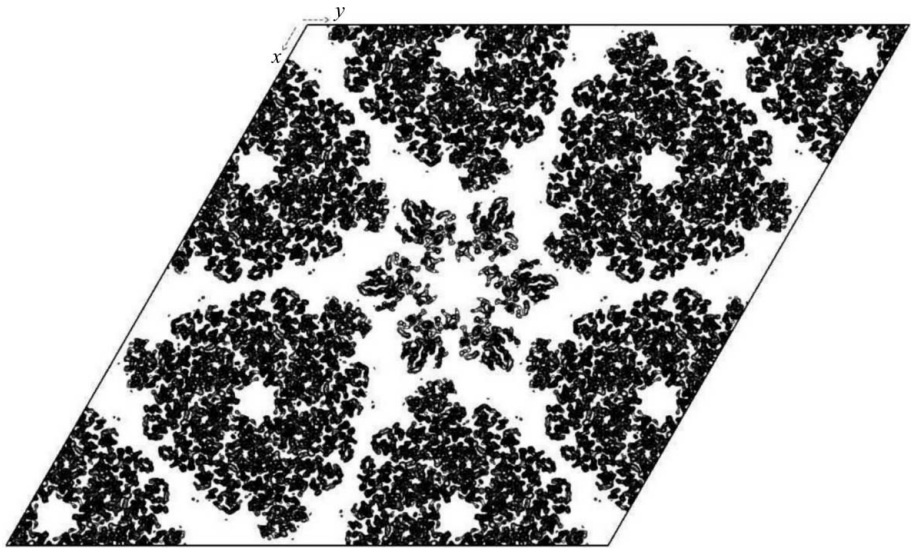

Figure 3
Superposition of electron-density map sections 12–23 along z from a total of 83 ($-0.75 \leq x \leq 0.75$, $-0.75 \leq y \leq 0.75$, $0 \leq z \leq 1$) calculated with *FFT* (Collaborative Computational Project, Number 4, 1994) using the *SOLOMON*-optimized (Abrahams & Leslie, 1996) phases after the *SHARP* (de La Fortelle & Bricogne, 1997) calculations. The contours were drawn at 1.0 and 2.0 map r.m.s. units. This figure was prepared with the programs *NPO* and *XPLOT84DRIVER* (Collaborative Computational Project, Number 4, 1994).

A major difficulty in this study has been the observation of polymorphism in both native and SeMet RuvBL1 crystals: the $P6_3$ form seemed to result from the $P6$ form by doubling of the unit-cell edge c, whereas a and b remain practically unchanged. Data analysis suggested that this transformation resulted from some sort of perturbation of the $P6$ form which gave rise to the appearance of a new set of reflections with odd l index (in $P6_3$) but which were systematically much weaker than those with even l index (the same set that is observed for the $P6$ form). This had severe implications in terms of the diffraction data statistics (Table 1) from the $P6_3$ crystals. Moreover, the average intensity of the odd l-index reflections in comparison with the even l-index ones varied from crystal to crystal. More recently (data not shown), we were able to determine that this effect was a random phenomenon caused by the cryoprotecting solution (2 *M* sodium malonate pH 6.0). Although the crystals were grown in sodium malonate, the effect of this salt upon flash-cooling ranged from harmless ($P6$ crystal form) to inducing a rearrangement of the crystal contacts with doubling of unit-cell edge c and space-group change to $P6_3$ and in extreme cases destroying the long-range order of the crystals such that only diffraction to very low resolution (*e.g.* 6–7 Å) could be observed. We were able to establish that the addition of 5% PEG 400 was sufficient to remove the $P6$ to $P6_3$ transformation, although a sufficiently long exposure (longer than 1 min, but variable upon the crystal size and quality) of the RuvBL1 crystals to the cryoprotecting solution still resulted in a degradation of their diffraction quality.

Finally, radiation damage was also a serious problem hindering this work. Significant radiation damage was detected in both the ID14-EH2 and ID29 data sets (Table 1) as an increasing B value as a function of batch number (*i.e.* exposure time). In order to minimize this problem, the ID14-4 data set was collected using the inverse-beam geometry and indeed the structure could be solved from it. However, inflection point and low-energy remote data sets measured from the same crystal failed to improve the quality of the initial phases and therefore precluded the application of the MAD data, which we believe would have provided significantly better starting phases and electron-density maps.

We thank Elzbieta Wiecko, Anja Wegg and Norbert Otto for help and advice with protein purification and Volker Badock for confirming that more than 95% of the methionine residues are replaced by selenomethionines in the SeMet derivative of RuvBL1.

References

Abrahams, J. P. & Leslie, A. G. W. (1996). *Acta Cryst.* D**52**, 30–42.
Altschul, S. F., Madden, T. L., Schaffer, A. A., Zhang, J., Zhang, Z., Miller, W. & Lipman, D. J. (1997). *Nucleic Acids Res.* **25**, 3389–3402.
Bauer, A., Chauvet, S., Huber, O., Usseglio, F., Rothbacher, U., Aragnol, D., Kemler, R. & Pradel, J. (2000). *EMBO J.* **19**, 6121–6130.
Berman, H. M., Westbrook, J., Feng, Z., Gilliland, G., Bhat, T. N., Weissig, H., Shindyalov, I. N. & Bourne, P. E. (2000). *Nucleic Acids Res.* **28**, 235–242.
Collaborative Computational Project, Number 4 (1994). *Acta Cryst.* D**50**, 760–763.
Dugan, K. A., Wood, M. A. & Cole, M. D. (2002). *Oncogene*, **21**, 5835–5843.
Evans, G. & Pettifer, R. (2001). *J. Appl. Cryst.* **34**, 82–86.
Feng, Y., Lee, N. & Fearon, E. R. (2003). *Cancer Res.* **63**, 8726–8734.
Ikura, T., Ogryzko, V. V., Grigoriev, M., Groisman, R., Wang, J., Horikoshi, M., Scully, R., Qin, J. & Nakatani, Y. (2000). *Cell*, **102**, 463–473.
Jonsson, Z. O., Dhar, S. K., Narlikar, G. J., Auty, R., Wagle, N., Pellman, D., Pratt, R. E., Kingston, R. & Dutta, A. (2001). *J. Biol. Chem.* **276**, 16279–16288.
Jonsson, Z. O., Jha, S., Wohlschlegel, J. A. & Dutta, A. (2004). *Mol. Cell*, **16**, 465–477.
Kabsch, W. (1993). *J. Appl. Cryst.* **26**, 795–800.
Kanemaki, M., Makino, Y., Yoshida, T., Kishimoto, T., Koga, A., Yamamoto, K., Yamamoto, M., Moncollin, V., Egly, J. M., Muramatsu, M. & Tamura, T. (1997). *Biochem. Biophys. Res. Commun.* **235**, 64–68.
La Fortelle, E. de & Bricogne, G. (1997). *Methods Enzymol.* **276**, 472–494.
Leslie, A. G. W. (1992). *Jnt CCP4/ESF–EACBM Newsl. Protein Crystallogr.* **26**.
Makino, Y., Kanemaki, M., Kurokawa, Y., Koji, T. & Tamura, T. (1999). *J. Biol. Chem.* **274**, 15329–15335.
Matthews, B. W. (1968). *J. Mol. Biol.* **33**, 491–497.
Neuwald, A. F., Aravind, L., Spouge, J. L. & Koonin, E. V. (1999). *Genome Res.* **9**, 27–43.
Niwa, H., Tsuchiya, D., Makyio, H., Yoshida, M. & Morikawa, K. (2002). *Structure*, **10**, 1415–1423.
Otwinowski, Z. & Minor, W. (1997). *Methods Enzymol.* **276**, 307–326.
Pape, T. & Schneider, T. R. (2004). *J. Appl. Cryst.* **37**, 843–844.
Perrakis, A., Morris, R. & Lamzin, V. S. (1999). *Nature Struct. Biol.* **6**, 458–463.

Putnam, C. D., Clancy, S. B., Tsuruta, H., Gonzalez, S., Wetmur, J. G. & Tainer, J. A. (2001). *J. Mol. Biol.* **311**, 297–310.
Schneider, T. R. & Sheldrick, G. M. (2002). *Acta Cryst.* D**58**, 1772–1779.
Sheldrick, G. M. (2002). *Z. Kristallogr.* **217**, 644–650.
Shen, X., Mizuguchi, G., Hamiche, A. & Wu, C. (2000). *Nature (London)*, **406**, 541–544.
Tsaneva, I. R., Muller, B. & West, S. C. (1993). *Proc. Natl Acad. Sci. USA*, **90**, 1315–1319.
Wood, M. A., McMahon, S. B. & Cole, M. D. (2000). *Mol. Cell*, **5**, 321–330.
Yamada, K., Kunishima, N., Mayanagi, K., Ohnishi, T., Nishino, T., Iwasaki, H., Shinagawa, H. & Morikawa, K. (2001). *Proc. Natl Acad. Sci. USA*, **98**, 1442–1447.